Geomechanics and Engineering, *Vol. 15, No. 4 (2018) 947-955*
DOI: https://doi.org/10.12989/gae.2018.15.4.947

Three-dimensional simplified slope stability analysis by hybrid-type penalty method

Kiyomichi Yamaguchi[*1], Norio Takeuchi[1a] and Eisaku Hamasaki[2b]

[1]*Graduate school of Engineering and Design, Hosei University, Tokyo 162-0843, Japan*
[2]*Adovantechnology Co., Ltd, Sendai 980-0013, Japan*

(Received May 17, 2017, Revised December 15, 2017, Accepted January 1, 2018)

Abstract. In this study, we propose a three-dimensional simplified slope stability analysis using a hybrid-type penalty method (HPM). In this method, a solid element obtained by the HPM is applied to a column that divides the slope into a lattice. Therefore, it can obtain a safety factor in the same way as simplified methods on the slip surface. Furthermore, it can obtain results (displacement and strain) that cannot be obtained by conventional limit equilibrium methods such as the Hovland method. The continuity condition of displacement between adjacent columns and between elements for each depth is considered to incorporate a penalty function and the relative displacement. For a slip surface between the bottom surface and the boundary condition to express the slip of slope, we introduce a penalty function based on the Mohr-Coulomb failure criterion. To compute the state of the slip surface, an r-min method is used in the load incremental method. Using the result of the simple three-dimensional slope stability analysis, we obtain a safety factor that is the same as the conventional method. Furthermore, the movement of the slope was calculated quantitatively and qualitatively because the displacement and strain of each element are obtained.

Keywords: hybrid-type penalty method; slope stability; slip surface; safety factor; displacement; strain

1. Introduction

Simplified methods for evaluating slope stability include the limit equilibrium method (LEM; Razdolsky *et al*. 2005, Deng *et al*. 2015, Xiao *et al*. 2015), the finite element method (FEM; Ji and Liao 2014, Tschuchnigg *et al*. 2015a, b), the combined LEM and FEM method (Sloan 2013), the rigid FEM (Liu and Zhao 2013), and the distinct element method (DEM; Liu *et al*. 2014). In addition, the influence of the three-dimensional slope shape is discussed when dealing with the three-dimensional model (Gao *et al*. 2013, 2016, Michalowski and Nadukuru 2013, Zhang *et al*. 2013, Shen and Karakus 2014, Lim *et al*. 2015). Furthermore, methods using new numerical analysis such as the particle method have been studied for investigating slope failure with large deformation behavior (Peng *et al*. 2015).

The authors proposed a three-dimensional simplified slope stability analysis method based on the rigid-body spring model (RBSM; Kawai 1977, Takeuchi and Kawai 1997, Yagi and Takeuchi 2015). The input data of this method is equivalent to a simplified method such as the Hovland method and Janbu method. The purpose of this method was to grasp the qualitative slope movement because the safety factor of the slope with the conventional simplified method cannot obtain information regarding the deformation condition of the slope.

In recent years, methods that use the deformation condition have been discussed such as using the deformation and strain state of the slope to evaluate the slope stability (Murata *et al*. 2014). For such evaluation methods, it is necessary to grasp the quantitative deformation condition, and a calculation method was proposed using the Spencer method and the Newmark method.

On the other hand, the present authors and others have developed the hybrid-type penalty method (HPM; Takeuchi *et al*. 2001, Ohki and Takeuchi 2005, Mihara and Takeuchi 2005, 2007, Vardanyan and Takeuchi 2008, Takeuchi *et al*. 2009, Yagi and Takeuchi 2011, Fujiwara *et al*. 2015) as a discretization method based on the principle of hybrid-type virtual work equation (Washizu 1968). In this method, the same discretization limit analysis as RBSM can be performed. In addition, the accuracy of the displacement solution is equivalent to FEM with constant strain element (Mihara and Takeuchi 2005, Ohki and Takeuchi 2005). This assumes the same degree of freedom as the discontinuous deformation analysis (DDA; Ohnishi *et al*. 2013). However, DDA mainly deals with a mass of discrete bodies and is therefore used for the collapse analysis of a rock mass having many discontinuity planes (Jiang *et al*. 2013, Jiang and Zheng 2015).

On the other hand, HPM is considered applicable to phenomena such as landslides and full-layer avalanches because it can express approximately continuous models using a penalty function. In addition, as compared with the previous study of three-dimensional simplified slope

∗Corresponding author, Graduate Student
E-mail: kiyomichi.yamaguchi.9r@stu.hosei.ac.jp
[a]Professor
E-mail: takeuchi@hosei.ac.jp
[b]Ph.D.

Copyright © 2018 Techno-Press, Ltd.
http://www.techno-press.org/?journal=gae&subpage=7
ISSN: 2005-307X (Print), 2092-6219 (Online)

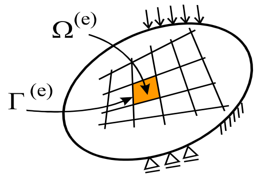

Fig. 1 Subdomains $\Omega^{(e)}$ and the boundary $\Gamma^{(e}$

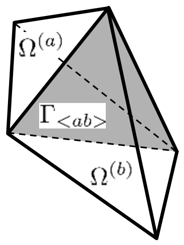

Fig. 2 Common boundary $\Gamma_{<ab>}$ between subdomains $\Omega^{(a)}$ and $\Omega^{(b)}$

stability analysis methods using RBSM, the accuracy of the displacement solution is improved as the strain results are obtained.

In this paper, we propose a simple method to evaluate the slope stability by applying HPM to the previous study of three-dimensional simplified slope stability analysis method using RBSM. Finally, we describe the features of the obtained solution using numerical examples.

2. Summary of the HPM

2.1 Hybrid-type virtual work equation

Fig. 1 shows that domains Ω consist of *M* subdomains $\Omega^{(e)}$ with the closed boundary $\Gamma^{(e)}$.

$$\Omega = \bigcup_{e=1}^{M} \Omega^{(e)} \text{ where } \Omega^{(r)} \bigcap \Omega^{(q)} = 0 (r \neq q) \tag{1}$$

Then the virtual work equation is represented by the sum of each subdomains as follows

$$\sum_{e=1}^{M}\left(\int_{\Omega^{(e)}} \boldsymbol{\sigma} : grad\, \delta\mathbf{u} dV - \int_{\Omega^{(e)}} \mathbf{f} \cdot \delta\mathbf{u} dV - \int_{\Gamma^{(e)}} \hat{\mathbf{t}} \cdot \delta\mathbf{u} dS\right) = 0 \tag{2}$$

$$^{\forall}\delta\mathbf{u} \in V, V \overset{def.}{=} \left\{\delta\mathbf{u} : \Omega \to R^3 \mid \delta\mathbf{u}\,|_{\Gamma_u} = 0\right\} \tag{3}$$

We use $\Gamma_{<ab>}$ to denote the common boundary between two subdomains $\Omega^{(a)}$ and $\Omega^{(b)}$, which are adjoined, as shown in Fig. 2.

The boundary $\Gamma_{<ab>}$ satisfies the following conditions

$$\Gamma_{<ab>} = \Gamma^{(a)} \bigcap \Gamma^{(b)} \tag{4}$$

In the principle of hybrid-type virtual work, the following equation represents the continuity condition on the boundary

$$\mathbf{u}^{(a)}_{<ab>} = \mathbf{u}^{(b)}_{<ab>} \quad \text{on} \quad \Gamma_{<ab>} \tag{5}$$

Here $\mathbf{u}^{(a)}_{<ab>}$ and $\mathbf{u}^{(b)}_{<ab>}$ represent the displacement on the boundary $\Gamma_{<ab>}$ with each subdomains $\Omega^{(a)}$ and $\Omega^{(b)}$, as shown in

$$\mathbf{u}^{(a)}_{<ab>} \overset{def.}{=} \mathbf{u}^{(a)}\,|_{\Gamma_{<ab>}}, \qquad \mathbf{u}^{(b)}_{<ab>} \overset{def.}{=} \mathbf{u}^{(b)}\,|_{\Gamma_{<ab>}} \tag{6}$$

The continuity condition of Eq. (5) can be represented in the following form with the Lagrange multiplier

$$H_{ab} \overset{def.}{=} \delta \int_{\Gamma_{<ab>}} \boldsymbol{\lambda} \cdot \left(\mathbf{u}^{(a)}_{<ab>} - \mathbf{u}^{(b)}_{<ab>}\right) dS \tag{7}$$

Eq. (7) is introduced into the virtual work equation (2). Then, the hybrid-type virtual work equation is obtained.

The number of common boundaries of the subdomain is *N*, and hybrid-type virtual work equation is represented as

$$\begin{aligned} &\sum_{e=1}^{M}\left(\int_{\Omega^{(e)}} \boldsymbol{\sigma} : grad\, \delta\mathbf{u} dV - \int_{\Omega^{(e)}} \mathbf{f} \cdot \delta\mathbf{u} dV - \int_{\Gamma^{(e)}} \mathbf{t} \cdot \delta\mathbf{u} dS\right) \\ &- \sum_{s=1}^{N}\left(\delta \int_{\Gamma_{<s>}} \boldsymbol{\lambda} \cdot \left(\mathbf{u}^{(a)}_{<ab>} - \mathbf{u}^{(b)}_{<ab>}\right) dS\right) = 0 \end{aligned} \tag{8}$$

2.2 Displacement field

The HPM assumes independent displacement fields in each subdomain. In this study, it assumes a first-order displacement field as shown Fig. 3 and the expression

$$\mathbf{u}^{(e)} = \mathbf{N}^{(e)}_d \mathbf{d}^{(e)} + \mathbf{N}^{(e)}_\varepsilon \boldsymbol{\varepsilon}^{(e)} \tag{9}$$

where each coefficient is

$$\mathbf{u}^{(e)} = \lfloor u, v, w \rfloor^t \tag{10}$$

$$\mathbf{d}^{(e)} = \lfloor u_0, v_0, w_0, \theta_0, \phi_0, \chi_0 \rfloor^t \tag{11}$$

$$\boldsymbol{\varepsilon}^{(\mathbf{e})} = \lfloor \varepsilon_{x0}, \varepsilon_{y0}, \varepsilon_{z0}, \gamma_{xy0}, \gamma_{yz0}, \gamma_{zx0} \rfloor^t \tag{12}$$

$$\mathbf{N}^{(e)}_d = \begin{bmatrix} 1 & 0 & 0 & 0 & Z^{(e)} & -Y^{(e)} \\ 0 & 1 & 0 & -Z^{(e)} & 0 & X^{(e)} \\ 0 & 0 & 1 & Y^{(e)} & -X^{(e)} & 0 \end{bmatrix} \tag{13}$$

$$\mathbf{N}^{(e)}_\varepsilon = \begin{bmatrix} X^{(e)} & 0 & 0 & Y^{(e)}/2 & 0 & Z^{(e)}/2 \\ 0 & Y^{(e)} & 0 & X^{(e)}/2 & Z^{(e)}/2 & 0 \\ 0 & 0 & Z^{(e)} & 0 & Y^{(e)}/2 & X^{(e)}/2 \end{bmatrix} \tag{14}$$

$$X^{(e)} = x - x_0, \quad Y^{(e)} = y - y_0, \quad Z^{(e)} = z - z_0 \tag{15}$$

Here $\mathbf{d}^{(e)}$ and $\boldsymbol{\varepsilon}^{(e)}$ are the rigid displacement and the strain at arbitrary points in the domain, and $\mathbf{N}_d^{(e)}$ and $\mathbf{N}_\varepsilon^{(e)}$ are the coefficient matrices related to the coordinates.

Therefore, the displacement field in HPM has the degree of freedom of strain and its gradient in addition to the rigid displacement and rigid rotation at arbitrary point in the domain. The conventional displacement-type FEM uses the

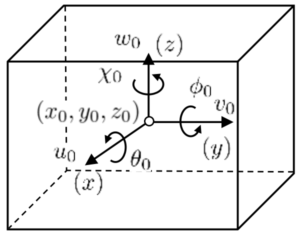

Fig. 3 Displacement field in each subdomain

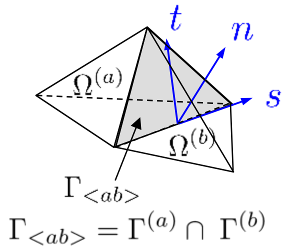

Fig. 4 The surface force on the boundary in subdomains

apexes of the element to the degree of freedom. However, HPM does not share the displacement at the apex because the displacement field is represented by the parameter at an arbitrary point in each domain.

2.3 Relative displacement and Lagrange multiplier

The physical interpretation of the Lagrange multiplier means the surface force on the boundary. The surface force on the boundary $\Gamma_{<ab>}$ in subdomains $\Omega^{(a)}$ and $\Omega^{(b)}$ as shown in Fig. 4 can be represented as in the following equation with the relative displacement $\delta_{<ab>}$ and the penalty matrix $\mathbf{k}$

$$\boldsymbol{\lambda}_{<ab>} = \mathbf{k} \cdot \boldsymbol{\delta}_{<ab>} \tag{16}$$

By using the matrix form, Eq. (16) is represented as follows

$$\begin{Bmatrix} \lambda_{s<ab>} \\ \lambda_{t<ab>} \\ \lambda_{n<ab>} \end{Bmatrix} = \begin{bmatrix} k_s & 0 & 0 \\ 0 & k_t & 0 \\ 0 & 0 & k_n \end{bmatrix} \begin{Bmatrix} \delta_{s<ab>} \\ \delta_{t<ab>} \\ \delta_{n<ab>} \end{Bmatrix} \tag{17}$$

Here $\delta_{s<ab>}$, $\delta_{t<ab>}$, and $\delta_{n<ab>}$, are the relative displacement for the tangential and normal direction on the element boundary $\Gamma_{<ab>}$. Similarly, $\lambda_{s<ab>}$, $\lambda_{t<ab>}$and $\lambda_{n<ab>}$ are the Lagrange multiplier for the tangential and normal direction and k_s, k_t and k_n are the penalty function for the tangential and normal direction. When the penalty matrix is a sufficiently large value, the displacement continuity is approximately represented on the boundary.

2.4 Discretization equation

We introduce the relation of Eqs. (9) and (16) to Eq. (8); finally, we obtain the following discretization equation

$$\mathbf{KU} = \mathbf{P} \tag{18}$$

Here $\mathbf{K}$ and $\mathbf{P}$ are

$$\mathbf{K} = \sum_{e=1}^{M} \mathbf{K}^{(e)} + \sum_{s=1}^{N} \mathbf{K}_{<s>} \tag{19}$$

$$\mathbf{P} = \sum_{e=1}^{M} \mathbf{W}_f^{(e)} + \sum_{e=1}^{M} \mathbf{P}^{(e)} \tag{20}$$

where $\mathbf{K}^{(e)}$ is the stiffness matrix of the element (e) and $\mathbf{K}_{<s>}$ is the continuity condition on the element boundary <s>.

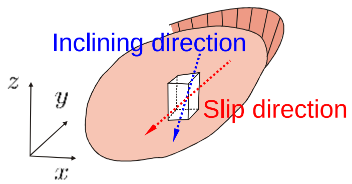

(a) The modeling slope

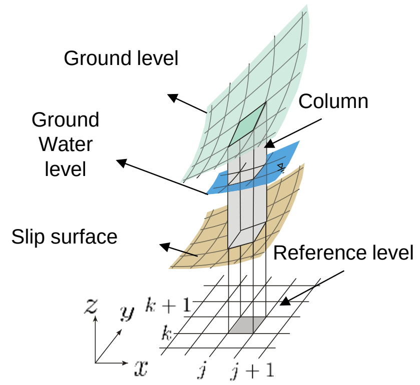

(b) The division by the lattice

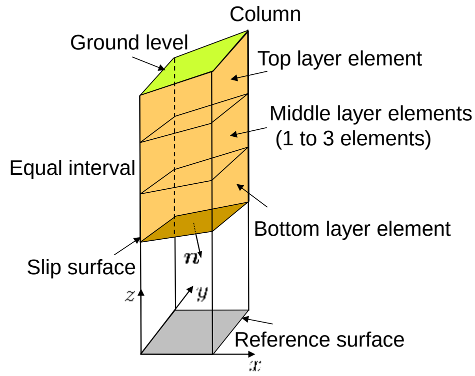

(c) The division of the column

Fig. 5 Method of element division with a column

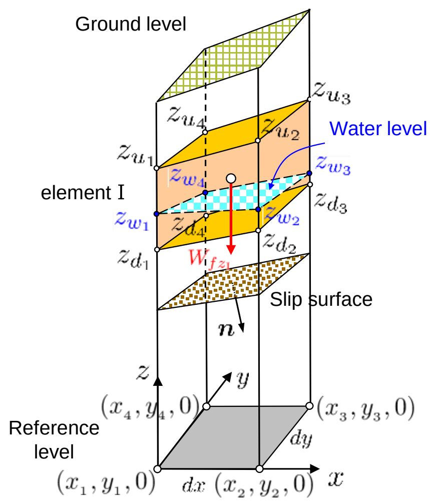

Fig. 6 The weight of the column

3. Modeling for three-dimensional simplified slope stability analysis

3.1 Method of element division with column

In this study, the stability analysis of HPM uses the same input parameter as the conventional simplified method. Therefore, we apply the modeling method that divides the slope into a lattice and that calculates with an assumed slip surface to the same as conventional simplified method as shown in Fig. 5(b). When the model is the slope as shown in Fig. 5(a), it is divided into the column by the x and y direction of the lattice as shown in Fig. 5(b).

Moreover, we divide this column in the z direction as shown in Fig. 5(c), because HPM can consider the elastic deformation. We divide the column with equal interval to the top layer element, the bottom layer element, and the middle layer elements. We increase the number of middle layer elements depending on the accuracy of calculation. However, the material uses the same stiffness in each column, because the purpose of this method is simplified slope stability analysis that we can use with the same input parameter as the conventional simplified method. In this study, we use the average of the stiffness of the column.

3.2 Weight of the column

The weight of the column uses the average of unit weight in each column. When the groundwater level is considered as shown in Fig. 6, this part uses the submerged weight.

In the case of element I in Fig. 6, the average height of upper, lower, and water level are

$$\text{Upper:}\quad H_u = \frac{z_{u1}+z_{u2}+z_{u3}+z_{u4}}{4} \tag{21}$$

$$\text{Lower:}\quad H_d = \frac{z_{d1}+z_{d2}+z_{d3}+z_{d4}}{4} \tag{22}$$

$$\text{Water level:}\quad H_w = \frac{z_{w1}+z_{w2}+z_{w3}+z_{w4}}{4} \tag{23}$$

The weight of an element is calculated as follows

$$H_w \le H_d,\quad W_{fz1} = \gamma_t \cdot (H_u - H_d)\cdot dxdy \tag{24}$$

$$H_w \ge H_d,\quad W_{fz1} = \gamma_{sub} \cdot (H_u - H_d)\cdot dxdy \tag{25}$$

$$H_d < H_w < H_u,$$

$$W_{fz1} = \gamma_{sub}\cdot(H_w - H_d)\cdot dxdy + \gamma_t\cdot(H_u - H_w)\cdot dxdy \tag{26}$$

where γ_t is the wet weight and γ_{sub} is the submerged weight.

3.3 Seismic load

We treat the seismic load as a static problem by using the design horizontal seismic coefficient. Fig. 7 shows the state of the column using the seismic load.

In this study, the weight of the element I is W_I, and the designed horizontal seismic coefficient is k_h. The seismic load is obtained as

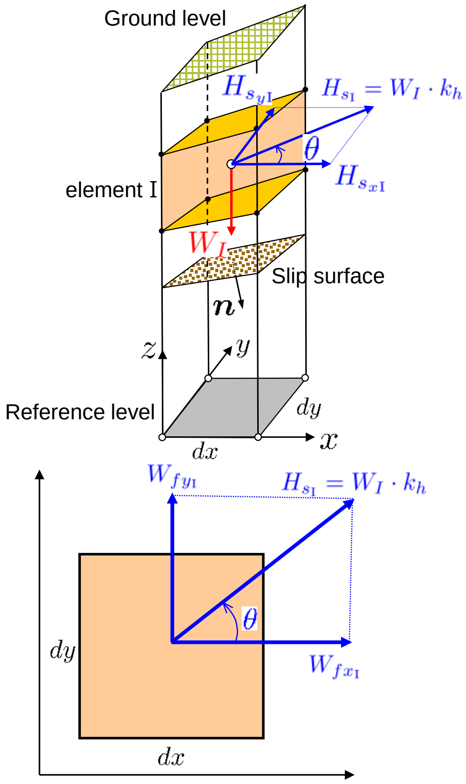

Fig. 7 The seismic load

$$H_{s1} = W_I \cdot k_h \tag{27}$$

The seismic load decomposes in the x-direction and y-direction as follows

$$W_{fx1} = H_{s1}\cdot\cos\theta \tag{28}$$

$$W_{fy1} = H_{s1}\cdot\sin\theta \tag{29}$$

4. Discretization for three-dimensional simplified slope stability analysis

4.1 Continuity condition of the column on the x-side surface

As shown in Fig. 8, we consider the contact situation of a column for the x-direction.

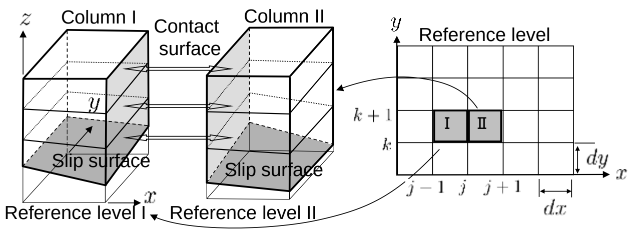

Fig. 8 The continuity condition of a column for the x-direction

It is assumed to connect for each of the layers, and the relative displacement of element I and II are obtained as

$$\boldsymbol{\delta}_{<\text{I}\cdot\text{II}>} = \mathbf{B}_{<\text{I}\cdot\text{II}>}\mathbf{U}_{<\text{I}\cdot\text{II}>} \tag{30}$$

where $\boldsymbol{\delta}_{<\text{I}\cdot\text{II}>}$ is the relative displacement, $\mathbf{U}_{<\text{I}\cdot\text{II}>}$ is the degree of freedom of elements I and II, and $\mathbf{B}_{<\text{I}\cdot\text{II}>}$ is the coefficient matrix.

The Lagrange multiplier $\boldsymbol{\lambda}_{<\text{I}\cdot\text{II}>}$ for elements I and II is represented as

$$\boldsymbol{\lambda}_{<\text{I}\cdot\text{II}>} = \mathbf{k}\,\boldsymbol{\delta}_{<\text{I}\cdot\text{II}>} \tag{31}$$

The penalty matrix $\mathbf{k}$ is

$$\mathbf{k} = \begin{bmatrix} k_s & 0 & 0 \\ 0 & k_t & 0 \\ 0 & 0 & k_n \end{bmatrix} \tag{32}$$

k_n is for the normal direction, k_s and k_t are for the shear direction.

In the case of the x-direction, the penalty matrix $\mathbf{k}$ is

$$\mathbf{k} = \mathbf{k}_{\text{x-side}} = \begin{bmatrix} \dfrac{E'}{(1+\nu)dx} & 0 & 0 \\ 0 & \dfrac{E'}{(1+\nu)dx} & 0 \\ 0 & 0 & \dfrac{(1+\nu)E'}{(1-2\nu)(1+\nu)dx} \end{bmatrix} \tag{33}$$

Here, we assume that the penalty function is p, and E' is assumed as

$$E' = E \times p \tag{34}$$

Therefore, the continuity condition of the side for the x-direction is discretized as

$$H_{\text{x-side}} = -\int_{\Gamma_{<ab>}} \mathbf{B}^t_{<\text{I}\cdot\text{II}>}\mathbf{k}_{\text{x-side}}\mathbf{B}_{<\text{I}\cdot\text{II}>}d\Gamma\,\mathbf{U}_{<\text{I}\cdot\text{II}>} \tag{35}$$

4.2 Continuity condition of a column on the y-side surface

We consider the continuity condition of a column for the y-direction as shown in Fig. 9.

This concept of the continuity condition is the same as in the x-direction. Therefore, in the case of the y-direction, the penalty matrix $\mathbf{k}$ is

$$\mathbf{k} = \mathbf{k}_{\text{y-side}} = \begin{bmatrix} \dfrac{E'}{(1+\nu)dy} & 0 & 0 \\ 0 & \dfrac{E'}{(1+\nu)dy} & 0 \\ 0 & 0 & \dfrac{(1+\nu)E'}{(1-2\nu)(1+\nu)dy} \end{bmatrix} \tag{36}$$

Finally, the continuity condition of the side for the y-direction is discretized as follows

$$H_{\text{y-side}} = -\int_{\Gamma_{<ab>}} \mathbf{B}^t_{<\text{I}\cdot\text{II}>}\mathbf{k}_{\text{y-side}}\mathbf{B}_{<\text{I}\cdot\text{II}>}d\Gamma\,\mathbf{U}_{<\text{I}\cdot\text{II}>} \tag{37}$$

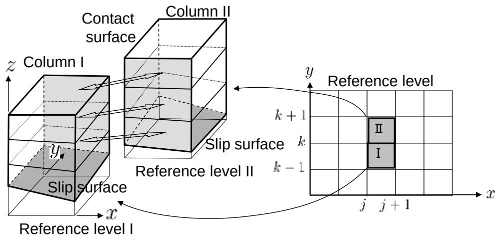

Fig. 9 The continuity condition of a column for the y-direction

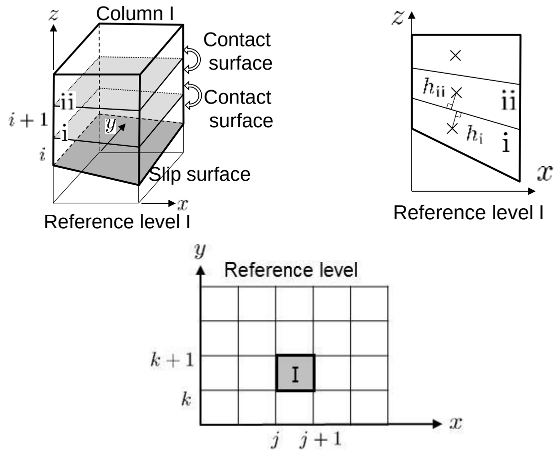

Fig. 10 The continuity condition of the column for the upper and lower surface

4.3 Continuity condition of column on upper and lower surface

As shown in Fig. 10, the column is divided to at least three parts: the top layer, the bottom layer, and the middle layer(s). The division method uses equal intervals and it ignores the stratum and groundwater.

In the case of the contact surface for the side as in Sections 4.1 and 4.2, the coordinate transformation for the normal direction is not necessary to obtain the relative displacement, because the contact surface is parallel to the y-z plane and x-z plane. However, in the case of the upper and lower surface, it is not parallel to the x-y plane. Thus, the coordinate transformation is necessary.

In this case, the relative displacement is obtained with the coordinate transformation matrix $\mathbf{R}_{<\text{i}\cdot\text{ii}>}$ as follows

$$\boldsymbol{\delta}_{<\text{i}\cdot\text{ii}>} = \mathbf{R}_{<\text{i}\cdot\text{ii}>}\mathbf{B}_{<\text{i}\cdot\text{ii}>}\mathbf{U}_{<\text{i}\cdot\text{ii}>} \tag{38}$$

The Lagrange multiplier $\boldsymbol{\lambda}_{<\text{i}\cdot\text{ii}>}$ for elements I and II is represented as

$$\boldsymbol{\lambda}_{<\text{i}\cdot\text{ii}>} = \mathbf{k}_{\text{vertical}}\boldsymbol{\delta}_{<\text{i}\cdot\text{ii}>} \tag{39}$$

where the penalty matrix $\mathbf{k}_{\text{vertical}}$ is

$$\mathbf{k}_{\text{vertical}} = \begin{bmatrix} \dfrac{E'}{(1+\nu)h} & 0 & 0 \\ 0 & \dfrac{E'}{(1+\nu)h} & 0 \\ 0 & 0 & \dfrac{(1+\nu)E'}{(1-2\nu)(1+\nu)h} \end{bmatrix} \tag{40}$$

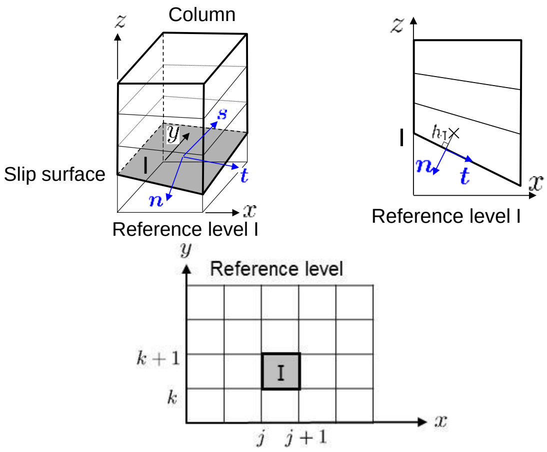

Fig. 11 The continuity condition of the column for the slip surface

Here, $h = h_{\mathrm{i}} + h_{\mathrm{ii}}$ is the average of height of upper and lower surface and E' is used as the relation of Eq. (34).

Therefore, the continuity condition of the upper and lower surface is discretized as follows

$$H_{\mathrm{vertical}} = -\int_{\Gamma_{<ab>}} \mathbf{B}^{t}_{<\mathrm{i\text{-}ii}>} \mathbf{k}_{\mathrm{vertical}} \mathbf{B}_{<\mathrm{i\text{-}ii}>} d\Gamma\, \mathbf{U}_{<\mathrm{i\text{-}ii}>} \tag{41}$$

4.4 Continuity condition of the column on the slip surface

As shown in Fig. 11, we consider the continuity condition regarding the slip surface.

To obtain the direction of the slip surface, we introduce the concept of an isoparametric element to the slip surface as

$$z(x,y) = \sum_{\alpha=1}^{4} N_{\alpha}(\xi,\eta) z_{\alpha} \tag{42}$$

In this case, the normal vector **n** and shear vector **s** and **t** on the slip surface are obtained as

$$\mathbf{n} = \frac{1}{\sqrt{1+\left(\frac{\partial z}{\partial x}\right)^2+\left(\frac{\partial z}{\partial y}\right)^2}}\left(\frac{\partial z}{\partial x}\mathbf{i}+\frac{\partial z}{\partial y}\mathbf{j}-\mathbf{k}\right) = n_x\mathbf{i}+n_y\mathbf{j}+n_z\mathbf{k} \tag{43}$$

$$\mathbf{s} = \frac{1}{\sqrt{1+\left(\frac{\partial z}{\partial y}\right)^2}}\left(\mathbf{j}+\frac{\partial z}{\partial y}\mathbf{k}\right) = s_y\mathbf{j}+s_z\mathbf{k} \tag{44}$$

$$\mathbf{t} = \frac{1}{\sqrt{1+\left(\frac{\partial z}{\partial x}\right)^2}}\left(\mathbf{i}+\frac{\partial z}{\partial x}\mathbf{k}\right) = t_x\mathbf{i}+t_z\mathbf{k} \tag{45}$$

The relative displacement of the slip surface is obtained with the displacement of column $\mathbf{U}^{(I)}$ as follows

$$\boldsymbol{\delta}_{\mathrm{slip}} = \mathbf{R}_{\mathrm{slip}}\mathbf{B}_{\mathrm{slip}}\mathbf{U}^{(I)} \tag{46}$$

Here the coordinate transformation matrix $\mathbf{R}_{\mathrm{slip}}$ is represented with the relation Eq. (43)-(45) as follows

$$\mathbf{R}_{\mathrm{slip}} = \begin{bmatrix} 0 & s_y & s_z \\ t_x & 0 & t_z \\ n_x & n_y & n_z \end{bmatrix} \tag{47}$$

The Lagrange multiplier of the slip surface is

$$\boldsymbol{\lambda}_{\mathrm{slip}} = \mathbf{k}_{\mathrm{slip}}\boldsymbol{\delta}_{\mathrm{slip}} \tag{48}$$

where the penalty matrix $\mathbf{k}_{\mathrm{slip}}$ is

$$\mathbf{k}_{\mathrm{slip}} = \begin{bmatrix} \frac{E'}{(1+\nu)h_I} & 0 & 0 \\ 0 & \frac{E'}{(1+\nu)h_I} & 0 \\ 0 & 0 & \frac{(1+\nu)E'}{(1-2\nu)(1+\nu)h_I} \end{bmatrix} \tag{49}$$

where E' uses the coefficient of the slip surface

$$E' = E_{\mathrm{slip}} \tag{50}$$

Therefore, the continuity condition of the slip surface is discretized as

$$H_{\mathrm{slip}} = -{}^{t}\delta\mathbf{U}^{(I)} \int_{\Gamma_{<ab>}} \mathbf{B}^{t}_{\mathrm{slip}}\mathbf{k}_{\mathrm{slip}}\mathbf{B}_{\mathrm{slip}} d\Gamma\, \mathbf{U}^{(I)} \tag{51}$$

4.5 Strain energy in each element and total energy of model

As shown in Section 2, the HPM can be used to evaluate the element stiffness.

As shown in Fig. 12, in the case of element I, its strain $\boldsymbol{\varepsilon}^{(I)}$ and stress $\boldsymbol{\sigma}^{(I)}$ are

$$\boldsymbol{\varepsilon}^{(I)} = \mathbf{B}^{(I)}\mathbf{U}^{(I)} \tag{52}$$

$$\boldsymbol{\sigma}^{(I)} = \mathbf{D}^{(I)}\boldsymbol{\varepsilon}^{(I)} \tag{53}$$

where $\mathbf{B}^{(I)}$ is the matrix that is the relation between the strain and the displacement and $\mathbf{D}^{(I)}$ is the structural matrix of a general three-dimensional elastic body

$$\mathbf{B}^{(I)} = \begin{bmatrix} 0&0&0&0&0&0&1&0&0&0&0&0 \\ 0&0&0&0&0&0&0&1&0&0&0&0 \\ 0&0&0&0&0&0&0&0&1&0&0&0 \\ 0&0&0&0&0&0&0&0&0&1&0&0 \\ 0&0&0&0&0&0&0&0&0&0&1&0 \\ 0&0&0&0&0&0&0&0&0&0&0&1 \end{bmatrix} \tag{54}$$

$$\mathbf{D}^{(I)} = \frac{E}{(1+\nu)(1-2\nu)} \begin{bmatrix} 1-\nu & \nu & \nu & 0 & 0 & 0 \\ \nu & 1-\nu & \nu & 0 & 0 & 0 \\ \nu & \nu & 1-\nu & 0 & 0 & 0 \\ 0 & 0 & 0 & (1-\nu)/2 & 0 & 0 \\ 0 & 0 & 0 & 0 & (1-\nu)/2 & 0 \\ 0 & 0 & 0 & 0 & 0 & (1-\nu)/2 \end{bmatrix} \tag{55}$$

In this case, the element stiffness is represented as

$$W_{\mathrm{column}} = {}^{t}\delta\mathbf{U}^{(I)} \int_{\Omega^{(I)}} {}^{t}\mathbf{B}^{(I)}\mathbf{D}^{(I)}\mathbf{B}^{(I)} d\Omega\, \mathbf{U}^{(I)} \tag{56}$$

Therefore, the total energy is obtained with Eqs. (35), (37), (41), (51), and (56) as follows

$$V = W_{\text{column}} + H_{\text{x-side}} + H_{\text{y-side}} + H_{\text{vertical}} + H_{\text{slip}} \qquad (57)$$

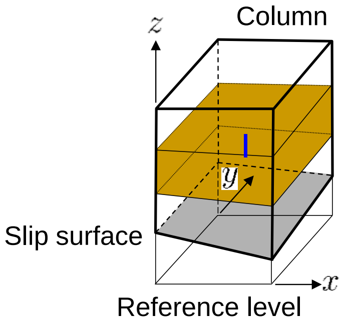

Fig. 12 The element stiffness of column

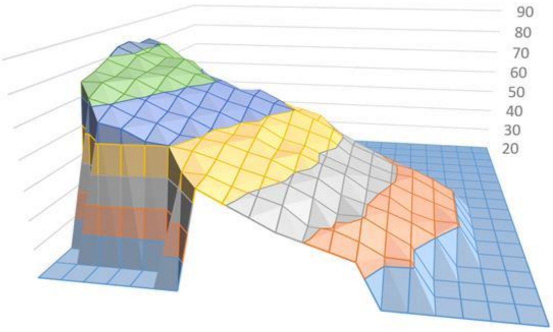

(a) The ground level

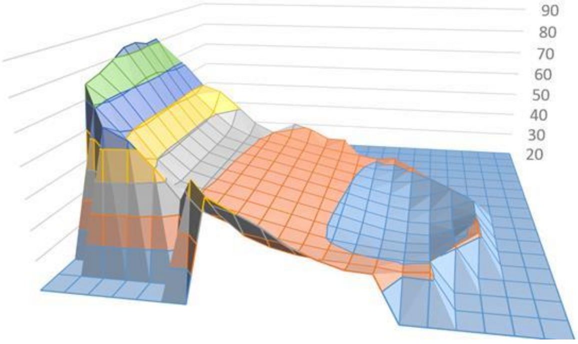

(b) The slip surface

Fig. 13 The numerical model

Table 1 The shape size

The number of divisions for x *nx*	16
The number of divisions for y *ny*	20
The number of divisions for z *nz*	3
The width of divisions for x (m) *dx*	10
The width of divisions for y (m) *dy*	10

Table 2 The material parameters

Unit of weight (kN/m^3) γ_t	18
Cohesion (kN/m^2) C	4.22
Internal frictional angle (°) ϕ	22
Elastic coefficient (GPa) E	1
Poisson ratio ν	0.2

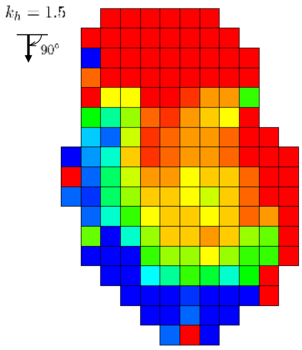

(a) The elastic analysis Fs = 1.104

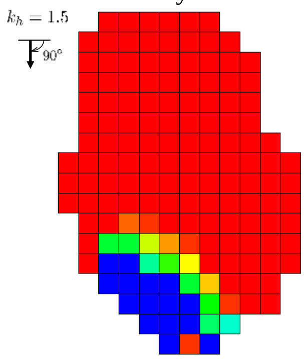

(b) The nonlinear analysis Fs = 1.155

Fig. 14 The local safety factor

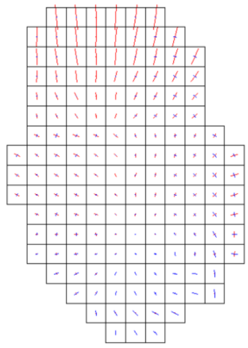

(a) The elastic analysis

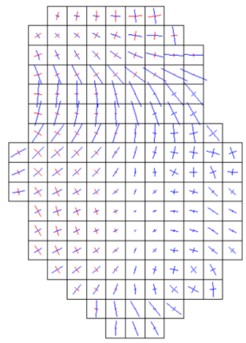

(b) The nonlinear analysis

Fig. 15 The principal strain

5. Numerical example

5.1 Numerical model

The numerical model is shown in Fig. 13: (a) represents the ground level and (b) represents the assumed slip surface.

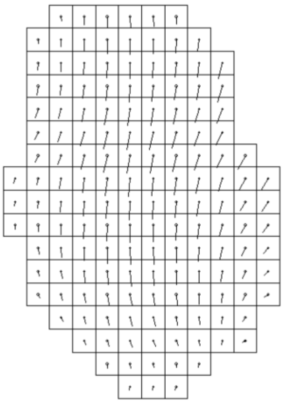

(a) The elastic analysis

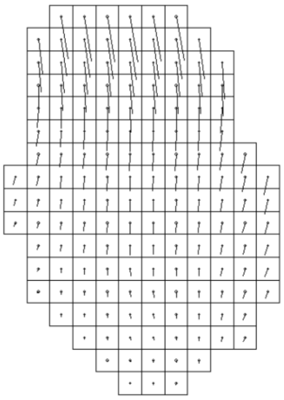

(b) The nonlinear analysis

Fig. 16 The displacement vector

The number and width of divisions are shown in Table 1.

The material parameters are shown in Table 2. To compute the state of the slip surface, we use a penalty function based on the Mohr-Coulomb failure criterion as the yield criterion on the slip surface and an r-min method as the load incremental method (Takeuchi *et al*. 2001, Ohki and Takeuchi 2005). And HPM obtains directly the normal and shear surface force on the slip surface. Therefore the safety factor is calculated by these surface force that are considered the Mohr-Coulomb failure criterion.

Regarding the assumed slip surface, the coefficient of the penalty function is assumed as follows

$$k_n = \frac{(1+\nu)E}{(1-2\nu)(1+\nu)h_I} \tag{58}$$

$$k_s = k_t = 100 \text{ MPa/m} \tag{59}$$

5.2 Result in a seismic load

Fig. 14 shows the safety factor at the slip surface when considering seismic load: (a) shows the elastic analysis result without the slip failure and (b) shows the nonlinear analysis result with the slip failure. The designed horizontal seismic coefficient is 1.5 in the y-direction.

Red lattice represents that the safety factor is 1 or less and blue lattice represents 2 or more. The total safety factor in the elastic analysis is 1.104 and in the nonlinear analysis is 1.155. The total safety factor of the elastic analysis is smaller than the nonlinear analysis. On the other hand, the local safety factor of the nonlinear analysis shows that the slip occurs over a wide area. The local safety factor of elastic analysis is less than 1. When the local safety factor approaches zero, there is the tendency that the total safety factor is reduced. This result confirms that tendency.

Regarding the comparison with stationary elastic analysis, the safety factor of this method is 1.767. On the other hand, with the modified Hovland method, the safety factor that calculated using the angle of the slip surface is 1.538, and the safety factor assuming that the entire slope slips downward is 2.188. The actual sliding direction is these mixed patterns, and the safty factor is between these values. On the other hand, the solution by proposed method is the value between these safety factors.

Regarding the calculation amount, the total number of degree of freedom is 5544 in the case of this model.

Therefore this method required 56 iterations of simultaneous equations with 5544 degrees of freedom for the elasto-plastic analysis. In the case of conventional simplified method, its calculation is one time.

Fig. 15 shows the principal strain at the ground level when considering seismic load.

Red vectors represent the tensile strain and blue vectors the compressive strain. The compressive strain occurs at the lower side in the elastic analysis. However, the large tensile strain occurs at the upper side because the slip does not occur in the elastic analysis. On the other hand, the compressive state is shown in the nonlinear analysis because the slip occurs at the upper side. Therefore, this change of strain state indicates the possibility to predict the sign of failure.

Fig. 16 shows the displacement at the ground level when considering seismic load.

The displacement at the upper side should be the largest by slip. However, it is smaller than in the central area in the elastic analysis. This is due to the unnatural constraint without slip. On the other hand, the displacement vector where the slip occurred is the largest in the nonlinear analysis. Moreover, the constraint state appeared in the area where the slip does not occur at the lower side.

6. Conclusions

In this paper, we proposed a three-dimensional simplified slope stability analysis by using HPM to obtain the strain and displacement. In conventional simplified method, the safety factor of maximum of inclining on slip surface at each column is obtained. And the safety factor may be less than 1 to calculate the safety factor by decomposing forces of column weight to direction of the slip surface. On the other hand, this method can obtain the safety factor of displacement direction. And the surface force on the slip surface moves on the failure surface because it is obtained by nonlinear analysis considering the Mohr-Coulomb failure criterion. Therefore the safety factor is not less than 1. And as mentioned the comparison with stationary elastic analysis, the solution of this method was obtained between solutions of the modified Hovland method. In addition this method makes it possible to obtain the change of strain and displacement before and after slip. Therefore, we can extend this model to the evaluation of the multidirectional stability by adding an evaluation of the deformation condition to the conventional slope stability analysis.

References

Deng, D.P., Zhao, L.H. and Li, L. (2015), "Limit equilibrium slope stability analysis using the nonlinear strength failure criterion", *Can. Geotech. J.*, **52**(5), 563-576.

Fujiwara, Y., Takeuchi, N., Shiomi, T., and Kambayashi, A. (2015), "Discrete crack modeling of RC structure using hybrid-type penalty method", *Comput. Concrete*, **16**(4), 587-604.

Gao, D.W., Zhang, F., Lei, G.H., Qin, H. and Qiu, Y. (2016), "Limit analysis of 3D rock slope stability with non-linear failure criterion", *Geomech. Eng.*, **10**(1), 59-76.

Gao, Y., Zhang, F., Lei, G.H., Li, D., Wu, Y. and Zhang, N. (2013), "Stability charts for 3D failures of homogeneous slopes", *J. Geotech. Geoenviron. Eng.*, **139**(9), 1528-1538.

Ji, J. and Liao, H.J. (2014), "Sensitivity-based reliability analysis of earth slopes using finite element method", *Geomech. Eng.*, **6**(6), 545-560.

Jiang, Q., Chen, Y., Zhou, C. and Yeung, M.C.R. (2013), "Kinetic energy dissipation and convergence criterion of discontinuous deformations analysis (DDA) for geotechnical engineering", *Rock Mech. Rock Eng.*, **46**(6), 1443-1460.

Jiang, W. and Zheng, H. (2015), "An efficient remedy for the false volume expansion of DDA when simulating large rotation", *Comput. Geotech.*, **70**, 18-23.

Kawai, T. (1977), "New element models in discrete structural analysis", *J. Soc. Naval Arch. Jap.*, **141**, 187-193.

Lim, K., Li, A.J. and Lyamin, A.V. (2015), "Three-dimensional slope stability assessment of two-layered undrained clay", *Comput. Geotech.*, **70**, 1-17.

Liu, F. and Zhao, J. (2013), "Limit analysis of slope stability by rigid finite-element method and linear programming considering rotational failure", *J. Geomech.*, **13**(6), 827-839.

Liu, Y., Li, H., Xiao, K., Li, J., Xia, X. and Liu, B. (2014), "Seismic stability analysis of a layered rock slope", *Comput. Geotech.*, **55**, 474-481.

Michalowski, R.L. and Nadukuru, S.S. (2013), "Three-dimensional limit analysis of slopes with pore pressure", *J. Geotech. Geoenviron. Eng.*, **139**(9), 1604-1610.

Mihara, R. and Takeuchi, N. (2005), "Material nonlinear analysis using hybrid-type penalty method assumed second-order displacement field", *Proceedings of the 7th International Conference on Analysis of Discontinuous Deformation*, Honolulu, Hawaii, U.S.A., December.

Mihara, R. and Takeuchi, N. (2007), "The three dimension models development by using linear displacement field in HPM", *Proceedings of APCOM'07 in Conjunction with EPMESC XI*, Kyoto, Japan, December.

Murata, M., Iijima, T., Mori, K., Nakamura, H., Ohashi, M. and Yamazaki, H. (2014), *Guideline for Design and Risk Evaluation against the Seismic Stability of the Ground Foundation and the Slope*, JNES-RE-Report Series 2013-2037, Japan Nuclear Energy Safety Organization.

Ohki, H. and Takeuchi, N. (2005), "Upper and lower bound solution with hybrid type penalty method", *Proceedings of the 7th International Conference on Analysis of Discontinuous Deformation*, Honolulu, Hawaii, U.S.A., December.

Ohnishi, Y., Koyama, T., Sasaki, T., Hagiwara, I., Miki, S., Shimauchi, T. and Nakamura, K. (2013), *Application of DDA and NMM to Practical Problems in Recent Insight*, in *Frontiers of Discontinuous Numerical Methods and Practical Simulations in Engineering and Disaster Prevention*, CRC Press, 29-42.

Peng, C., Wu, W., Yu, H.S. and Wang, C. (2015), "A SPH approach for large deformation analysis with hypoplastic constitutive model", *Acta Geotech.*, **10**(6), 703-717.

Razdolsky, A.G., Yankelevsky, D.Z. and Karinski, Y.S. (2005), "Analysis of slope stability based on evaluation of force balance", *Struct. Eng. Mech.*, **20**(3), 313-334.

Shen, J. and Karakus, M. (2014), "Three-dimensional numerical analysis for rock slope stability sing shear strength reduction method", *Can. Geotech. J.*, **51**(2), 164-172.

Sloan, S.W. (2013), "Geotechnical stability analysis", *Géotechnique*, **63**(7), 531-571.

Takeuchi, N. and Kawai, T. (1997) "Development of discrete limit analysis and its application to the solid mechanics", *Proceedings of the 2nd International Conference on Analysis of Discontinuous Deformation*, Kyoto, Japan, July.

Takeuchi, N., Ohki, H., Kambayashi, A. and Kusabuka, M. (2001), "Material non-linear analysis by using discrete model applied penalty method in hybrid displacement model", *Trans. Jap. Soc. Comput. Eng. Sci.*, 52-62.(in Japanese)

Takeuchi, N., Tajiri, Y. and Hamasaki, E. (2009), *Development of Modified RBSM for Rock Mechanics using Principle of Hybrid-Type Virtual Work*, in *Analysis of Discontinuous Deformation : New Developments and Applications*, Research Publishing Service, 395-403.

Tschuchnigg, F., Schweiger, H.F. and Sloan, S.W. (2015a), "Slope stability analysis by means of finite element limit analysis and finite element strength reduction techniques. Part I: Numerical studies considering non-associated plasticity", *Comput. Geotech.*, **70**, 169-177.

Tschuchnigg, F., Schweiger, H.F. and Sloan, S.W. (2015b), "Slope stability analysis by means of finite element limit analysis and finite element strength reduction techniques. Part II: Back analyses of a case history", *Comput. Geotech.*, **70**, 178-189.

Vardanyan, A.V. and Takeuchi, N. (2008), "Discrete analysis for plate bending problems by using hybrid-type penalty method", *Bull. Res. Center Comput. Multimed. Stud.*, **21**, 131-141.

Washizu. K (1968), *Variational Methods in Elasticity and Plasticity*, Pergamon Press, New York, U.S.A.

Xiao, S., Li, K., Ding, X. and Liu, T. (2015), "Numerical computation of homogeneous slope stability", *Comput. Intel. Neurosci.*, 1-10.

Yagi, T. and Takeuchi, N. (2011), *On Accuracy of Solution for Explicit and Implicit Dynamic Formation with Hybrid-Type Penalty Method*, in *Advances in Discontinuous Numerical Methods and Applications in Geomechanics and Geoengineering*, CRC Press, 419-425.

Yagi, T. and Takeuchi, N. (2015), "An explicit dynamic method of rigid bodies-spring model", *J. Comput. Meth.*, **12**(4), 1-15.

Zhang, Y., Chen, G., Zheng, L., Li, Y. and Zhuang, X. (2013), "Effects of geometries on three-dimensional slope stability", *Can. Geotech. J.*, **50**(3), 233-249.

CC